View metadata, citation and similar papers at core.ac.uk

brought to you by CORE

provided by Jagiellonian Univeristy Repository

⌘ *Author's Choice*

THE JOURNAL OF BIOLOGICAL CHEMISTRY VOL. 291, NO. 13, pp. 6872–6881, March 25, 2016

© 2016 by The American Society for Biochemistry and Molecular Biology, Inc. Published in the U.S.A.

Tuning of Hemes *b* Equilibrium Redox Potential Is Not Required for Cross-Membrane Electron Transfer*

Received for publication, December 22, 2015, and in revised form, February 2, 2016 Published, JBC Papers in Press, February 8, 2016, DOI 10.1074/jbc.M115.712307

Sebastian Pintscher, Patryk Kuleta, Ewelina Cieluch, Arkadiusz Borek, Marcin Sarewicz, and Artur Osyczka[1]

From the Department of Molecular Biophysics, Faculty of Biochemistry, Biophysics and Biotechnology, Jagiellonian University, 30-387 Kraków, Poland

In biological energy conversion, cross-membrane electron transfer often involves an assembly of two hemes *b*. The hemes display a large difference in redox midpoint potentials ($\Delta E_{m_}$b), which in several proteins is assumed to facilitate cross-membrane electron transfer and overcome a barrier of membrane potential. Here we challenge this assumption reporting on heme *b* ligand mutants of cytochrome bc_1 in which, for the first time in transmembrane cytochrome, one natural histidine has been replaced by lysine without loss of the native low spin type of heme iron. With these mutants we show that $\Delta E_{m_}$b can be markedly increased, and the redox potential of one of the hemes can stay above the level of quinone pool, or $\Delta E_{m_}$b can be markedly decreased to the point that two hemes are almost isopotential, yet the enzyme retains catalytically competent electron transfer between quinone binding sites and remains functional *in vivo*. This reveals that cytochrome bc_1 can accommodate large changes in $\Delta E_{m_}$b without hampering catalysis, as long as these changes do not impose overly endergonic steps on downhill electron transfer from substrate to product. We propose that hemes *b* in this cytochrome and in other membranous cytochromes *b* act as electronic connectors for the catalytic sites with no fine tuning in $\Delta E_{m_}$b required for efficient cross-membrane electron transfer. We link this concept with a natural flexibility in occurrence of several thermodynamic configurations of the direction of electron flow and the direction of the gradient of potential in relation to the vector of the electric membrane potential.

Redox midpoint potential (E_m) is a key property of any redox active cofactor in proteins. It regulates biological functions via thermodynamic and kinetic control of electron exchange reactions. Because these reactions must take place in a variety of cellular compartments, both outside and inside the biological membrane, the structures of redox proteins have evolved to meet physicochemical requirements of these various environments to achieve assemblies that secure functionally competent E_m values.

Within the group of cytochromes, molecular factors that modulate E_m include types of heme axial ligation (1–3). The residues that are most commonly recruited as axial ligands for the heme iron are His and/or Met (4). A binding of hemes *b* within the membranous proteins is accomplished by an assembly of transmembrane α-helices that provide His axial ligands for the heme-iron. In fact, the heme binding α-helix bundle represents a common motif of several bioenergetic complexes (5–7). It has even been used as a prototype to construct human-made versions of heme binding proteins (protein maquettes) (8–10).

The α-helix bundle can bind one or two hemes *b*. In several proteins, an assembly of two *b* type hemes, each facing different sides of the membrane, supports electron transfer across biological membranes crucial for energy conservation in many systems. Intriguingly, the two hemes differ largely in their redox midpoint potentials (the E_m difference, $\Delta E_{m_}$b, is typically in the range of 100 mV); however, the thermodynamic rationale behind the existence of $\Delta E_{m_}$b remains unclear. This is because no general rule for the direction of $\Delta E_{m_}$b with respect to the direction of the electric field generated by the membrane potential or the direction of physiological electron transfer is evident (Fig. 1).

The cytochrome *b* subunit of cytochrome bc_1 (mitochondrial complex III) is a well known example of a protein supporting cross-membrane electron transfer by using an assembly of two hemes *b*, named heme b_H and heme b_L, where subscripts H and L refer to high and low potential, respectively (for recent reviews see Refs. 11 and 12). During the catalytic cycle, the electron transfer from heme b_L to heme b_H connects the quinol oxidation site (Q_o)[2] and the quinone reduction site (Q_i). In addition, in dimeric structure of an enzyme, intermonomer electron transfer parallel to the membrane plane involving two hemes b_L is possible (13–16). In living cells, the cross-membrane electron flow from heme b_L to heme b_H may face the barrier of the membrane potential (Fig. 1*a*). Thus, the fact that electrons are transferred from the cofactor of lower E_m to the cofactor of higher E_m provided a basis for a general assumption that $\Delta E_{m_}$b is one of the factors that facilitate cross-membrane electron transfer and perhaps is important in overcoming the barrier of potential (17, 18). However, the contribution of

* This work was supported by The Wellcome Trust International Senior Research Fellowship (to A. O.). The Faculty of Biochemistry, Biophysics and Biotechnology of Jagiellonian University is a partner of the Leading National Research Center (KNOW) supported by the Ministry of Science and Higher Education. The authors declare that they have no conflicts of interest with the contents of this article.

⌘ *Author's Choice*—Final version free via Creative Commons CC-BY license.

[1] To whom correspondence should be addressed: Dept. of Molecular Biophysics, Faculty of Biochemistry, Biophysics and Biotechnology, Jagiellonian University, 7 Gronostajowa St., 30-387 Kraków, Poland. E-mail: artur.osyczka@uj.edu.pl.

[2] The abbreviations used are: Q_o, quinol oxidation site; Q_i, quinone reduction site; EPR, electron paramagnetic resonance spectroscopy; Q, quinone; QH_2, quinol; SQ, semiquinone.

Downloaded from http://www.jbc.org/ by guest on March 13, 2019

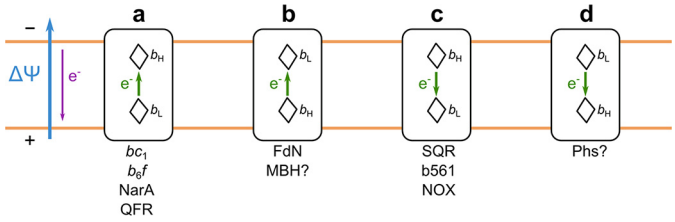

FIGURE 1. **Possible thermodynamic configurations for cross-membrane electron transfer in cytochromes *b*.** *a*, electron is transferred against ΔΨ and involves energetically favorable reduction of heme b_H by heme b_L. *b*, electron is transferred against ΔΨ and additionally involves energetically unfavorable reduction of heme b_L by heme b_H. *c*, energetically unfavorable reduction of heme b_L by heme b_H is facilitated by ΔΨ. *d*, energetically favorable reduction of heme b_H by heme b_L is additionally facilitated by ΔΨ. b_L and b_H denote low potential and high potential heme, respectively. The *blue arrow* refers to ΔΨ (membrane electric potential); the *purple arrow* indicates the direction of ΔΨ-induced electron transfer; and the *green arrows* indicate direction of electron transfer between hemes. Configuration *a* can be found in cytochrome bc_1 (11, 12), cytochrome b_6f (37), nitrate reductase A (*NarA*) (39, 40), and fumarate reductase (*QFR*) (41, 42); configuration *b* can be found in formate dehydrogenase N (*FdN*) (40, 43) and perhaps in membrane-bound [Ni-Fe] hydrogenase (*MBH*) (45, 46); configuration *c* can be found in succinate dehydrogenase (*SQR*) (47, 48), cytochromes b_{561} (*b561*) (52–54), and NADPH oxidase (*NOX*) (51); and configuration *d* probably exists in thiosulfate reductase (*Phs*) (55).

$\Delta E_{m\_}b$ to the overall electron flow has not been verified experimentally. Prerequisites for such verification are variants of cytochrome bc_1 with large changes in the E_m of hemes *b* and, consequently, large changes in $\Delta E_{m\_}b$. However, the mutations of cytochrome *b* tested so far either had a relatively small effect on the E_m of hemes *b* (19, 20) or resulted in the absence of the heme (21, 22).

Here we mutated the native bis-His coordination pattern for heme b_L and/or heme b_H into the His-Lys pattern, to our knowledge, providing the first His-Lys coordinated hemes *b* in a transmembrane protein. The hemes remain low spin as in a native enzyme but have markedly elevated E_m values and thus effectively modulate $\Delta E_{m\_}b$: an increase in the E_m of heme b_H by 50 mV increased $\Delta E_{m\_}b$ setting the E_m of heme b_H above the E_m of the quinone pool in the membrane, whereas an increase in the E_m of heme b_L by 155 mV decreased $\Delta E_{m\_}b$ to the point that the two hemes *b* were almost isopotential. This provided an unprecedented set of large changes in $\Delta E_{m\_}b$ for functional testing. The results offer a new perspective toward understanding the natural engineering of the cross-membrane electron transfer in cytochromes *b*.

Experimental Procedures

Bacterial Strains, Plasmids, and Growth Conditions—*Rhodobacter capsulatus* and *Escherichia coli* (HB101, DH5α) were grown in liquid or solid MPYE (mineral-peptone-yeast extract) and LB (Luria Bertani) media, at 30 and 37 °C, respectively, supplemented with appropriate antibiotics as needed. Respiratory growth of *R. capsulatus* strains was achieved at 30 °C in the dark under semiaerobic conditions. Photosynthetic growth abilities of mutants were tested on MPYE plates using anaerobic jars (GasPak™ EZ Anaerobe Container System; BD Biosciences) at 30 °C under continuous light. The *R. capsulatus* strains used were: pMTS1/MTRbc_1 which overproduces wild-type cytochrome bc_1 from the expression vector pMTS1 (contains a copy of pet*ABC* operon coding for all three subunits of cytochrome bc_1), and MTRbc_1 which is a pet*ABC* operon deletion background (23). The mutagenized pMTS1 derivatives were introduced to *R. capsulatus* MTRbc_1 via triparental crosses as described (23). Plasmid pPET1 (a derivative of pBR322 containing a wild-type copy of pet*ABC*) was used as a template for PCR and in some of the subcloning procedures.

Construction of Lys Mutants—Spontaneous Ps^+ revertant of the H212N mutant originally described in Ref. 22 was obtained on MPYE plate containing tetracycline after ~7 days of cultivation under photosynthetic conditions. The DNA sequence analysis of the plasmid DNA isolated from the revertant strain revealed a single base pair change replacing the mutated Asn into Lys at position 212 of cytochrome *b*. The XmaI/SfuI fragment containing the reversion (mutation H212K), and no other mutations was exchanged with its counterpart on expression vector pMTS1 carrying the wild-type copy of the pet*ABC* operon. Expression of this vector in the MTRbc_1 background strain confirmed that cells bearing single mutation H212K display the photosynthetically competent Ps^+ phenotype. The Ps^+ reversion H212K occurred also in the double mutant A181T/H212N cultivated on MPYE plate containing kanamycin (in this case H212N in the cytochrome *b* subunit was accompanied by a mutation A181T in cytochrome c_1 described originally in Ref. (24)). Because A181T/H212N, unlike original H212N, contained cytochrome *b* already equipped with the Strep-tag II attached to its carboxyl end, the plasmid obtained from the revertant of A181T/H212N was used to construct the mutants used in further analysis. First, the XmaI/SfuI fragment containing the reversion (H212K) and the sequence coding for Strep-tag II (ST), and no other mutations were exchanged with its counterpart on expression vector pMTS1 carrying the wild-type copy of the pet*ABC* operon. This created pMTS1-ST-H212K. Second, the same XmaI/SfuI fragment was cloned into pPET1 creating pPET1-ST-H212K. Mutation H198K and the double mutation H212K/H198K were constructed by the QuikChange site-directed mutagenesis kit from Stratagene using pPET1-ST (25) and pPET1-ST-H212K plasmids as templates, respectively, and the mutagenic forward H198K-F (5′-GGGCAGCAGATATTTCAGCGAGAAGAAGCGG-3′) and reverse H198K-R (5′-TTCTTCTCGCTGAAATATCTGCTG-CCCTTCG-3′) oligonucleotides. After sequencing, XmaI/SfuI fragments of pPET1 plasmids bearing the desired mutations, and no other mutations were exchanged with their wild-type counterparts in pMTS1. This created the plasmids pMTS1-ST-H198K and pMTS1-ST-H212K/H198K. Plasmids pMTS1-ST-H212K, pMTS1-ST-H198K, and pMTS1-ST-H212K/H198K were inserted into *R. capsulatus* MTRBC1 cells, creating mutants H212K, H198K, and H212K/H198K, respectively. These mutants are listed in Table 1. In each case, the presence of introduced mutations was confirmed by sequencing the plasmid DNA reisolated from the mutated *R. capsulatus* strains.

Isolation of Membranes and Proteins—Chromatophore membranes were isolated from *R. capsulatus* as described previously (26). The cytochrome bc_1 complexes were isolated from detergent-solubilized chromatophores by affinity chromatography using the procedure described previously (27). SDS-PAGE of purified complexes was performed as described before (28).

Downloaded from http://www.jbc.org/ by guest on March 13, 2019

Optical and EPR Spectroscopy—Optical spectra measurements of isolated complexes and determination of protein concentration were performed on UV-2450 Shimadzu spectrophotometer. Cytochrome bc_1 samples were suspended in 50 mM Tris, pH 8.0, 100 mM NaCl, 0.01% (m/m) dodecyl maltoside, and 1 mM EDTA, an appropriate amount of ferricyanide was added to fully oxidize complexes; then solid ascorbate and solid sodium dithionite were added to reduce samples, and spectra were recorded right after oxidation and after each step of reduction. Concentration of cytochrome bc_1 was determined as described (26). EPR measurements were performed on Bruker Elexys E580 spectrometer. X-band CW-EPR spectra of hemes were measured at 10 K, using SHQE0511 resonator combined with ESR900 Oxford Instruments cryostat unit, using 1.595 mT modulation amplitude, and 1.543 milliwatt of microwave power. For EPR measurements, cytochrome bc_1 samples were dialyzed against 50 mM Tris, pH 8.0, 100 mM NaCl, 20% glycerol (v/v), 0.01% (m/m) dodecyl maltoside, and 1 mM EDTA. Final concentration of cytochrome bc_1 in EPR samples was 50 μM. Antimycin A was used in 5-fold molar excess over the concentration of cytochrome bc_1.

Redox Potentiometry—Midpoint potentials of hemes *b* were determined by dark equilibrium redox titrations on chromatophores according to the method described in Ref. (29). Chromatophores were suspended in argon-equilibrated 50 mM MOPS buffer (pH 7.0) containing 100 mM KCl and 1 mM EDTA. Immediately before the titration, the following redox mediators were added: 100 μM tetrachlorohydroquinone, 100 μM 2,3,5,6-tetramethyl phenylenediamine (E_{m7} 260 mV), 100 μM 1,2-naphtoquinone-4-sulfonate (E_{m7} 210 mV), 100 μM 1,2-naphtoquinone (E_{m7} 130 mV), 50 μM phenazine methosulfate (E_{m7} 80 mV), 50 μM phenazine ethosulfate (E_{m7} 50 mV), 100 μM duroquinone (E_{m7} 5mV), 30 μM indigotrisulfonate ($E_{m7} = -90$ mV), 100 μM 2-hydroxy-1,4-napthoquinone ($E_{m7} = -152$ mV), 100 μM anthroquinone-2-sulfonate ($E_{m7} = -225$ mV), and 100 μM benzyl viologen ($E_{m7} = -374$ mV). Dithionite and ferricyanide were used to adjust ambient redox potential. During the titrations, samples of 150–200 μl were taken and transferred to EPR tubes anaerobically and frozen by immersion into cold ethanol. The E_{m7} values of hemes *b* were determined by fitting the amplitudes of appropriate EPR g_z transitions to the Nernst equation for one-electron couple (for WT, H212K, and H198K) or for two one-electron couples (in case of H212K/H198K mutant).

Flash-induced Electron Transfer Measurements—Measurements of flash-induced turnover kinetics of cytochrome bc_1 were performed on a home-built double wavelength time-resolved spectrophotometer as described in previous work (24). Chromatophores for measurements were suspended in 50 mM MOPS, pH 7.0, 100 mM KCl, 3.5 μM valinomycin, and redox mediators: 7 μM 2,3,5,6-tetramethyl-1,4-phenylenediamine, 1 μM phenazine methosulfate, 1 μM phenazine ethosulfate, 5.5 μM 1,2-naphthoquinone, and 5.5 μM 2-hydroxy-1,4-naphthoquinone (valinomycin and redox mediators were added immediately before the measurement). Dithionite and ferricyanide were used to adjust ambient redox potential. Inhibitors antimycin A and myxothiazol were used at final concentration of 7 μM. Transient hemes *b* reduction kinetics were followed at 560–570 nm (for WT and H198K) or 557–570 nm (for H212K and H212K/H198K). Transient hemes *c* oxidation and rereduction kinetics were followed at 550–540 nm. Single flash activation measurements were initiated by a short saturating flash (10 μs) from a xenon lamp, and multiple flash activation measurements were initiated by a series of short (10 μs) saturating flashes every 20 ms. In order to measure kinetics in the presence of the membrane potential, valinomycin was omitted. Rates of flash-induced heme *b* reduction were determined by fitting transient kinetics data to a single exponential equation.

Steady-state Kinetics Measurements—Steady-state enzymatic activities of cytochrome bc_1 complexes in chromatophores were determined spectroscopically by the decylubiquinol-dependent reduction of bovine heart cytochrome *c* (Sigma-Aldrich) as described before (23). Conditions used in assays were as follows: 50 mM Tris-HCl (pH 8), 100 mM NaCl, 20 μM decylubiquinol, 20 μM oxidized cytochrome *c*. Errors were calculated as standard deviation of the mean of nine measurements. Chromatophores were treated with KCN (final concentration in sample was 0.5 mM) before experiments. Decylubiquinol was obtained as described (30).

Results

His-Lys Ligation for Hemes b in a Low Spin State Is Possible in Transmembrane Cytochrome b—Changes in the coordination pattern of heme iron are expected to exert a large influence on the redox properties of hemes (1). Thus, to impose large shifts in E_m values of hemes *b* in cytochrome *b*, we created three variants in which one of the His ligands to heme iron was replaced by Lys (Lys mutants): single mutants H212K (for heme b_H) and H198K (for heme b_L) and the double mutant H212K/H198K combining both single mutations (Fig. 2*a*).

The mutated complexes contained all three catalytic subunits, as indicated by the SDS electrophoretic profiles (Fig. 3*a*). Optical (UV-visible), and electron paramagnetic resonance spectroscopy (EPR) showed that the mutants contained all redox active cofactors: heme c_1, hemes *b* (b_L and b_H) and 2Fe-2S cluster (Figs. 2*b* and 3, *b* and *c*). Although the spectral and redox properties of 2Fe-2S and heme c_1 remained unchanged in the mutants, the properties of hemes *b* were modified. We emphasize the results of EPR analysis (Fig. 2*b*), which in this case is most informative because, unlike UV-visible spectroscopy, it allows for a complete spectral separation of *g* transitions originating from each of the hemes *b*: in native enzyme $g = 3.78$ and 3.44, corresponding to g_z transition of heme b_L and heme b_H, respectively (31).

The mutationally imposed changes in ligation pattern resulted in the disappearance of the g_z transition of the targeted heme at the position characteristic for a native enzyme with concomitant appearance of new transitions at $g = 3.22$ and 3.15 (Fig. 2*b*, *black*). More specifically, these new transitions replaced $g = 3.78$ in H198K, $g = 3.44$ in H212K, and both $g = 3.78$ and 3.44 in the double mutant H212K/H198K. In general, these shifts reflect a lowering of the symmetry and changes from a highly axial to a more rhombic low spin heme (32). The new transitions $g = 3.22$ and 3.15 are assigned to g_z transitions of low spin hemes *b* coordinated by His-Lys. Support for this assignment comes from the differential effect of antimycin, an

Downloaded from http://www.jbc.org/ by guest on March 13, 2019

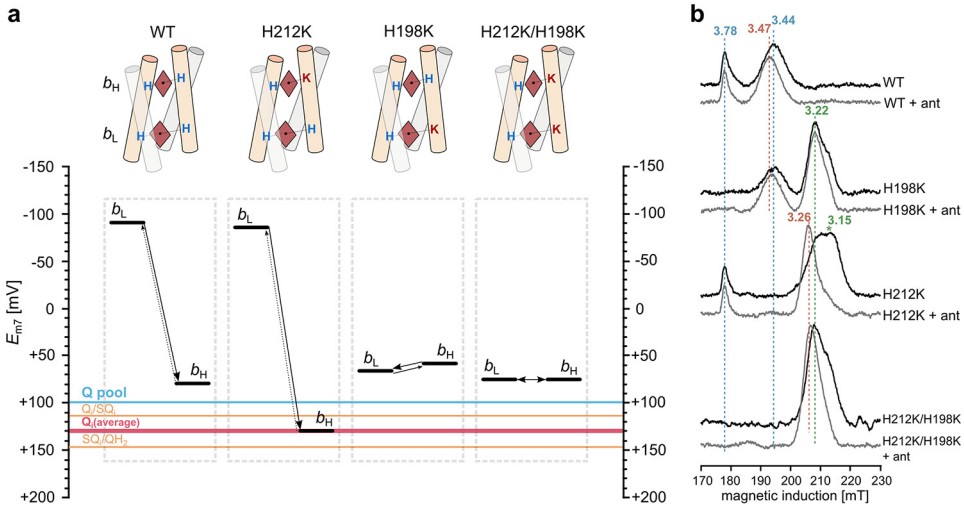

FIGURE 2. **His-Lys coordinated hemes *b* contain low spin heme iron and have markedly increased E_m.** *a*, schematic representation of four-helix bundles (*tubes*) binding two hemes *b* (*brown diamonds*) and introduced changes in the ligation pattern; *H* and *K* denote His and Lys ligands of heme iron, respectively. The respective E_m diagrams are shown *below* the schemes. *Black bars* refer to E_{m7} of hemes, the *blue line* indicates E_{m7} of Q pool, *orange lines* indicate calculated E_{m7}s of Q_i/SQ_i and SQ_i/Q_i couples (*upper* and *lower line*, respectively), and the *red line* indicates the resulting average E_{m7} of Q at the Q_i catalytic site. *b*, EPR spectra of hemes *b* in isolated complexes in the absence of inhibitors and presence of antimycin (*black* and *gray*, respectively). The *numbers* above the spectra and *dotted lines* denote values and positions of g_z transitions.

inhibitor that binds to the Q_i site in the proximity of heme b_H, and is known to affect the EPR spectrum of heme b_H (33). Antimycin clearly affects the $g = 3.22$ and 3.15 of heme b_H in H212K and H212K/H198K, whereas in H198K it has a weak or no effect (Fig. 2*b*, *gray*). In H212K/H198K, for which both hemes b_L and b_H contribute to 3.22 and 3.15 transitions, the effect of antimycin is intermediary between the largest and smallest effect seen in H212K and H198K, respectively.

His-Lys Coordinated Hemes b Have Markedly Elevated E_m, Effectively Modulating ΔE_m_b—Dark equilibrium redox titrations revealed that changing the ligation pattern from bis-His to His-Lys in hemes *b* leads to a significant increase in their E_m values. This increase reaches 50 mV for heme b_H in H212K and almost 160 mV for heme b_L in H198K (Fig. 4 and Table 1). At the same time, there was no significant change of E_m (only ~10 mV increase was observed in E_m for heme b_L in H212K or 20 mV decrease of E_m for heme b_H in H198K) in the heme that was not subject to modification in these mutants. A large increase in the E_m of just one heme (b_L or b_H) effectively modulated ΔE_m_b in those mutants (Fig. 2*a*). In H212K ΔE_m_b was increased, and E_m of heme b_H rose above the E_m of quinone pool in the membrane (34, 35). In H198K ΔE_m_b was decreased to the point that both hemes became almost isopotential. In H212K/H198K, both His-Lys ligated hemes showed E_m of ~72 mV. This means that only heme b_L elevated its E_m. Consequently, the ΔE_m_b in this mutant is similar to that of H198K.

Mutants with Large Changes in ΔE_m_b Are Functional in Vitro and in Vivo—Remarkably, all mutants showed the capability to grow under cytochrome bc_1-dependent photoheterotrophic conditions (*i.e.* exhibited the Ps^+ phenotype), which indicated that mutated cytochromes bc_1 are functional *in vivo* (Table 1 and Fig. 3, *d* and *e*). The functional competence of these mutants was confirmed by light-induced electron transfer measurements that allow monitoring of individual reactions associated with the catalytic cycle. In brief, these reactions include oxidation of quinol at the Q_o site, which delivers one electron to one cofactor chain (the c chain) consisting of a 2Fe-2S cluster, heme c_1 and heme c_2. The other electron is used to reduce heme b_L in a separate chain (the b chain), followed by cross-membrane electron transfer to heme b_H, which then reduces the occupant of the Q_i site.

The kinetic transients shown in Fig. 5 monitored changes in the oxidation state of heme b_H associated with electron transfer through the b chain. When the quinone (Q) pool is poised half-reduced before light activation (ambient potential of 100 mV at pH 7) (Fig. 5*a*), cytochrome bc_1 in native chromatophores and in the absence of any inhibitors displays a fast reduction of heme b_H followed by its fast reoxidation (WT, *black trace*). The reduction phase is mediated by an electron from the Q_o site, whereas the reoxidation phase results from electron transfer to the occupant of the Q_i site. In the presence of antimycin, the reoxidation phase is blocked, and heme b_H remains reduced within the time domain monitored in the experiment (WT, *red trace*). The rate of this reduction (measured at pH 7), as well as the rates measured at two other pH values (pH 6 and 9, which test conditions of different driving force provided by substrates) are listed in Table 1. All phases of the electron transfer described above and involving heme b_H (in the absence of any inhibitors and in the presence of antimycin) are observed in all Lys mutants, and the measured rates of heme b_H reduction at pH 6, 7, or 9 are only slightly lower than the corresponding rates in wild type (Fig. 5*a* and Table 1). This reveals a full competence of catalytic reactions of Q_o and Q_i sites in the mutants. We note the smaller amplitude of heme b_H reduction in the presence of antimycin in H212K mutant. This is an effect of a partial prereduction of this heme before activation, which is a consequence of an elevated E_m exceeding the E_m of the Q pool.

Kinetic competence of the mutants was also evident in the response of cytochrome bc_1 to multiple flash activation in both the absence and presence of membrane potential. In the absence of inhibitors, hemes *c* in native enzyme and H198K undergo several cycles of fast oxidation and rereduction (Fig.

Downloaded from http://www.jbc.org/ by guest on March 13, 2019

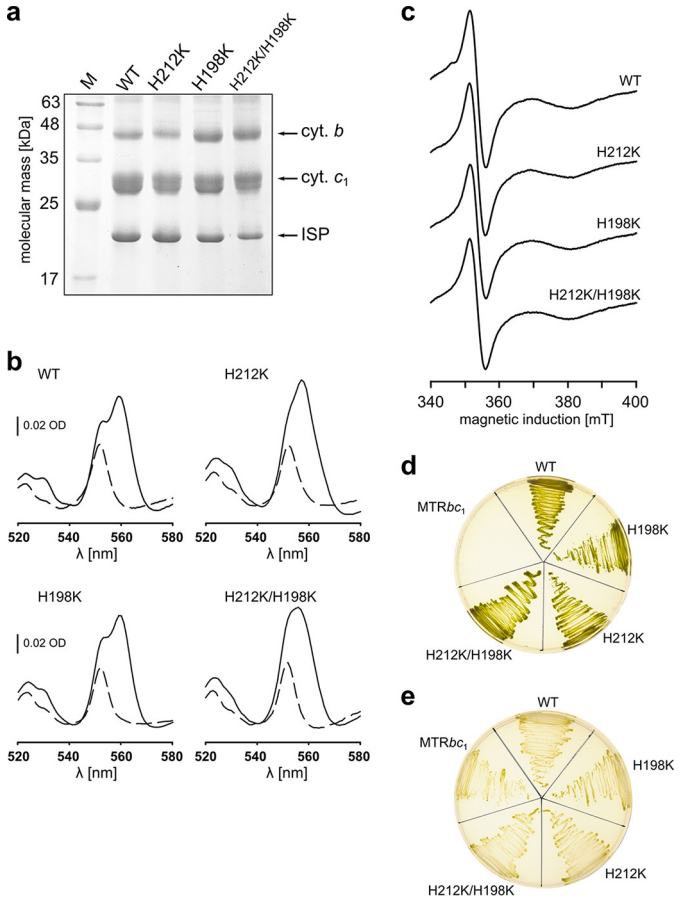

FIGURE 3. **SDS-PAGE profiles, spectral analyses, and growth capability of Lys mutants of cytochrome bc_1.** *a*, Coomassie Blue-stained SDS-PAGE profiles of complexes isolated from solubilized membranes. *b*, optical absorption spectra of isolated complexes: *dashed lines*, ascorbate-reduced samples; *solid lines*, dithionite-reduced samples. *c*, X-band CW-EPR spectra of reduced 2Fe-2S clusters present in samples of isolated complexes. Spectra were recorded at 20 K, 1.7 mT modulation amplitude, and 2.015 milliwatts of microwave power. *d*, photosynthetic growth under anaerobic conditions at pH 7. MTRbc_1 (*R. capsulatus* strain lacking cytochrome bc_1 operon) was used as negative control. *e*, heterotrophic growth in aerobic dark conditions (cytochrome bc_1-independent) at pH 7 was used as positive control.

6*a*, *black*), and hemes *b* undergo several cycles of fast reduction and reoxidation (Fig. 6*b*, *black*). As expected, antimycin impedes the rereduction phase of hemes *c* (Fig. 6*a*, *red*) and blocks the reoxidation phase of hemes *b* (Fig. 6*b*, *red*). The membrane potential diminishes the effectiveness of the rereduction of hemes *c* and reoxidation of hemes *b*, leading to partial accumulation of oxidized hemes *c* and reduced hemes *b*, but the magnitude of this effect in native enzyme and H198K is similar. In multiple flash experiments, H212K behaved similarly to H198K.

Enzymatic competence of the Lys mutants is evident in the measured steady-state turnover rates, which remain in good correlation with the results of light-induced electron transfer measurements. As listed in Table 1, the turnover rates in H212K or H198K single mutants and in H212K/H198K double mutant decrease by 20 and 40%, respectively, compared with WT. Clearly, all Lys mutants retain significant enzymatic activity.

Changes in $\Delta E_{m\_}b$ Affect Equilibria of Partial Reactions—Kinetic traces measured when the Q pool is fully oxidized before activation (ambient potential of 200 mV at pH 7) are compared in Fig. 5*b*. Under these conditions, the amount of quinol molecules after activation is limited, and consequently, approximately only one quinol is oxidized in every Q_o site. It follows that a difference between the level of reduction of heme b_H in the absence and presence of antimycin reports equilibration of electron between heme ${b_H}^{3+}/{b_H}^{2+}$ and quinone/semiquinone (Q/SQ) couples at the Q_i site. In native enzyme and H198K mutant, this difference is large, indicating that the electron resides mostly on semiquinone at the Q_i site (~80%). However, in H212K mutant, the amplitude of reduced heme b_H in the absence of inhibitors is significantly larger than in wild type. This indicates that equilibrium between heme ${b_H}^{3+}/{b_H}^{2+}$ and Q/SQ is shifted so that the electron resides mostly on heme b_H (at the expense of semiquinone). This shift is a consequence of an elevated E_m of heme b_H in H212K, which exceeds the E_m of Q/SQ at pH 7 (Fig. 2*a*).

Another way to monitor electron equilibration between heme b_H and the occupant of the Q_i site benefits from the occurrence of reverse reaction in the Q_i site (Fig. 5*c*). When the Q pool is fully oxidized before light activation, and the Q_o site is blocked by an inhibitor (myxothiazol), light-induced reduction of heme b_H reports electron transfer from quinol that entered the Q_i site to heme b_H. However, in a native enzyme, this reaction cannot be observed at pH 7 (Fig. 5*c*, *blue*), which seems consistent with the fact that E_m of heme b_H is lower than E_m of the Q pool. On the other hand, at this pH, the reverse electron transfer from Q_i site quinol to heme b_H is prominent in H212K (Fig. 5*c*, *blue*). Furthermore, the amplitude of heme b_H reduction in this reaction (*i.e.* in the presence of myxothiazol) is almost as large as the amplitude of heme b_H reduction in the absence of any inhibitor.

Equilibration of electrons between heme b_H and the occupant of the Q_i site in H212K mutant under the conditions described in Fig. 5 (*b* and *c*) allowed us to estimate the E_m values for the SQ/QH_2 and Q/SQ redox couples at the Q_i site at pH 7. The extent of forward reaction (electron transfer from heme b_H to Q) monitored in Fig. 5*b* will reflect the difference between the E_m of heme ${b_H}^{3+}/{b_H}^{2+}$ and the E_m of Q/SQ couples, whereas the extent of the reverse reaction (electron transfer from quinol to heme b_H) monitored in Fig. 5*c* will reflect the difference between the E_m of heme ${b_H}^{3+}/{b_H}^{2+}$ and the E_m of SQ/QH_2 couples. Based on these assumptions, and considering $E_{m7} = 130$ mV for heme b_H in an H212K mutant, we estimate values of E_{m7} for the Q/SQ couple to be ~114 mV, and E_{m7} for the SQ/QH_2 couple to be 147 mV. The average redox midpoint potential for Q/QH_2 (E_{m7} for Q/QH_2) is then 130 mV, which makes it isopotential with the ${b_H}^{3+}/{b_H}^{2+}$ couple in an H212K mutant and ~30 mV higher than the E_m of Q in the Q pool reported in the literature. The split in quinone redox couples defines the stability constant for SQ (35, 36); thus, our estimates of E_{m7} for Q/SQ and E_{m7} for SQ/QH_2 indicate the stability constant ($\log(K_s) = [E_{m(Q/SQ)} - E_{m(SQ/QH2)}]/60$) for SQ_i at the level of 3×10^{-1}.

Downloaded from http://www.jbc.org/ by guest on March 13, 2019

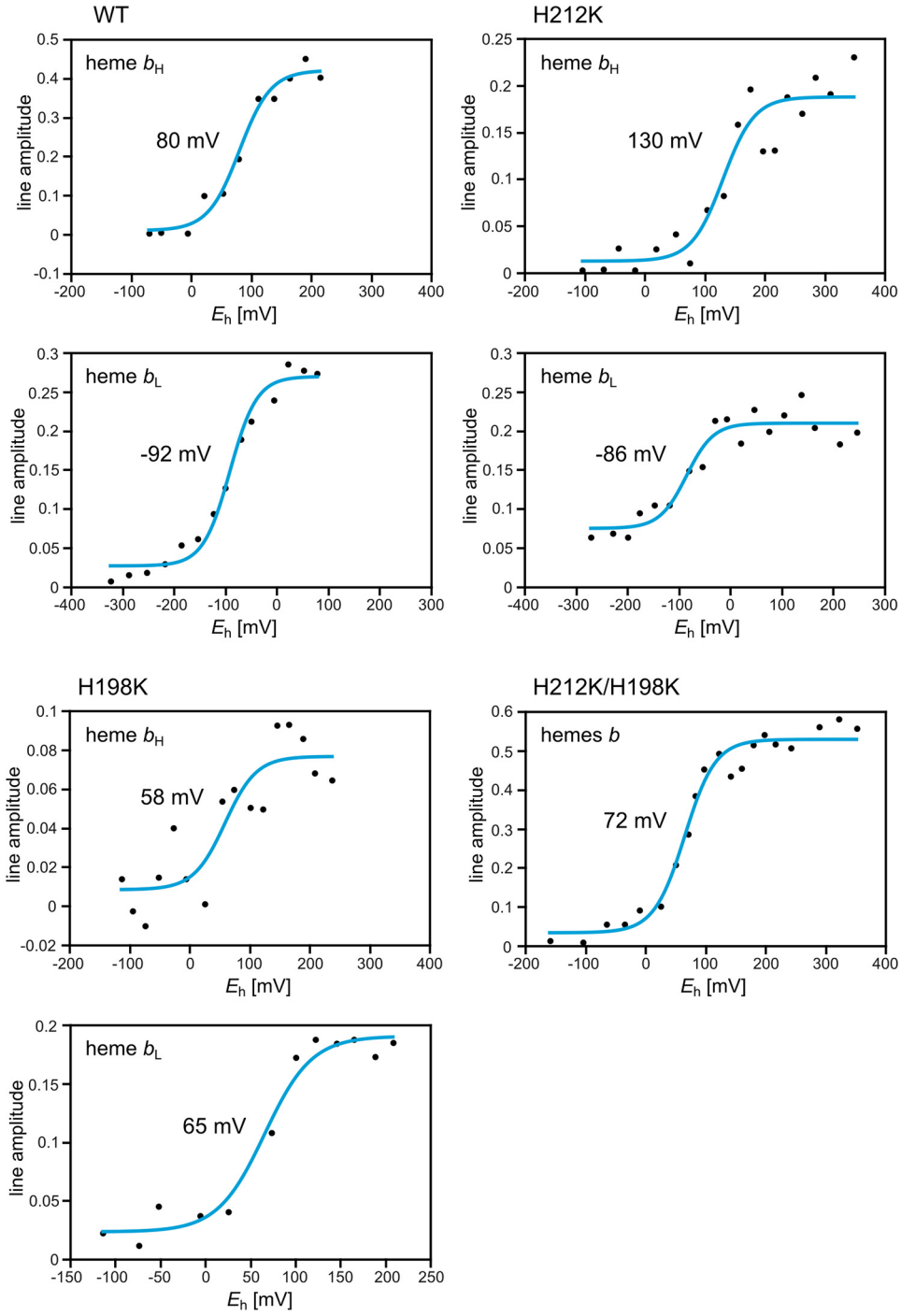

FIGURE 4. **Midpoint potentials of hemes *b* determined via EPR-monitored redox titrations.** Each *blue line* represents the Nernst titration curve. The respective E_m values are given in the middle of each plot. Titrations were performed on isolated chromatophores at pH 7.0. Amplitudes of heme b_L and heme b_H were monitored at respective *g* values: 3.78 and 3.44 in WT, 3.22 and 3.44 in H198K, 3.78 and 3.2 in H212K, and 3.2 in H212K/H198K.

TABLE 1
Selected properties of wild-type and Lys mutants

Form of bc_1	Phenotype	E_{m7}		EPR g_z value		Rates of hemes *b* reduction			Steady-state activity
		b_L	b_H	b_L	b_H (+antimycin)	pH 6	pH 7	pH 9	
		mV					s^{-1}		s^{-1}
WT	Ps^+	−92	80	3.78	3.44 (3.47)	566	1051	1791	149 ± 7
H212K	Ps^+	−86	130	3.78	3.22/3.15 (3.26)	479	822		121 ± 6
H198K	Ps^+	65	58	3.22	3.44 (3.47)	392	770	1506	118 ± 5
H212K/H198K	Ps^+	~72		~3.2	~3.2 (~3.24)	420	706	1548	91 ± 6

Downloaded from http://www.jbc.org/ by guest on March 13, 2019

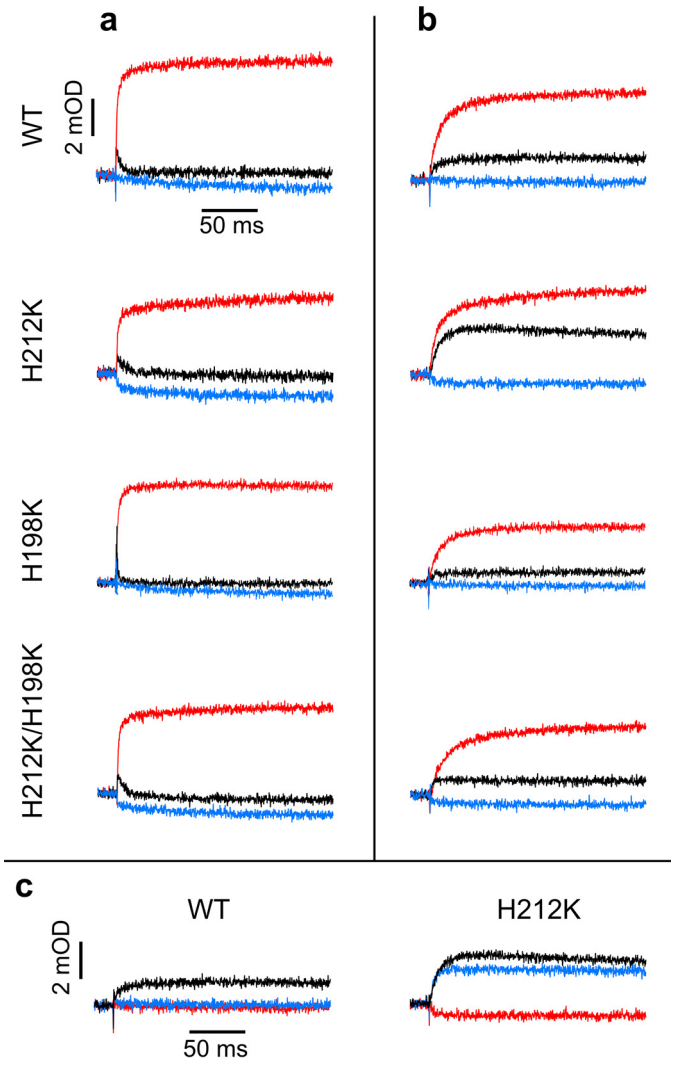

FIGURE 5. **Single flash-activated transients reveal fast heme *b* reduction and changes in equilibria of partial reactions in Lys mutants.** *a*, transients in the absence of inhibitor (*black*) after addition of antimycin (*red*) and subsequent addition of myxothiazol (*blue*) recorded at pH 7 and ambient potential of 100 mV (Q pool half-reduced). *b*, same as in *a*, except that ambient potential was 200 mV (Q pool oxidized). *c*, same as in *b*, except that the order of addition of inhibitors was inverted: antimycin (*red*) was subsequent to myxothiazol (*blue*). Transient hemes *b* reduction kinetics for WT and H198K were followed at 560–570 nm and for H212K and H212K/H198K at 557–570 nm.

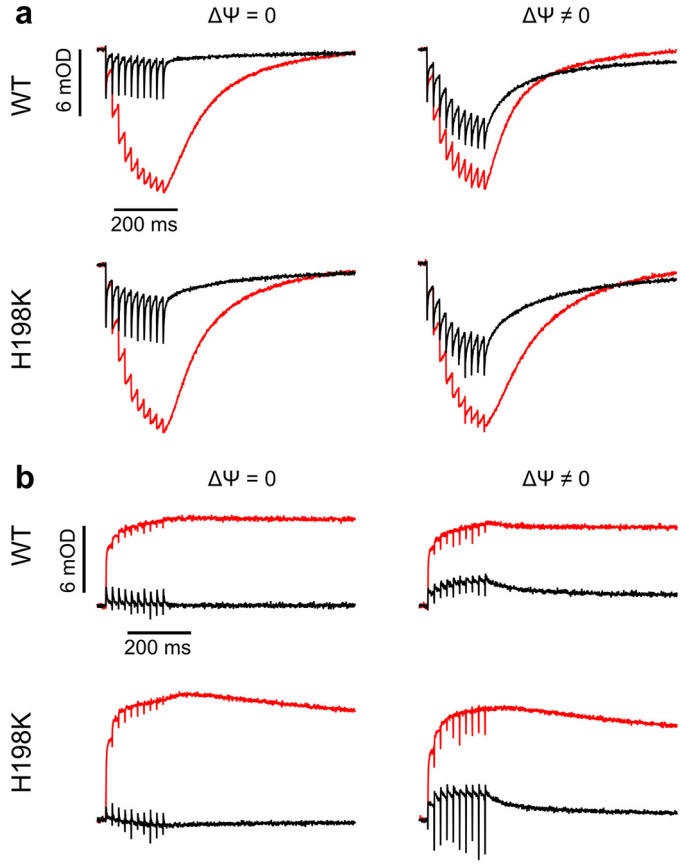

FIGURE 6. **Multiple flash-activated competence of enzyme with isopotential hemes *b* in the absence and presence of electric membrane potential.** *a*, transients for hemes *c* oxidation and rereduction in WT and H198K activated by 10 flashes separated by 20 ms in the absence of inhibitors (*black*) and in the presence of antimycin (*red*), in the absence ($\Delta\Psi = 0$) or presence ($\Delta\Psi \neq 0$) of the membrane potential, recorded at pH 7 and ambient potential of 100 mV. *b*, transients for hemes *b* recorded as in *a*.

Discussion

We have examined the effect of large changes in ΔG on electron transfer between hemes *b* in cytochrome bc_1. These changes were implemented by significant increases in the E_m values of the hemes, which came as a result of mutating the native bis-His coordination of the heme iron into the His-Lys coordination. Our results indicate that the natural difference in E_m values of the two hemes *b* ($\Delta E_{m_}$b) of 170 mV can be increased to 210 mV (in H212K) or diminished to almost 0 (in H198K and double mutant H212K/H198K), and the complex still remains functional *in vivo*, retaining the catalytically relevant electron transfer from the Q_o to Q_i sites measured *in vitro* under the absence or presence of membrane potential. The electron flow through cofactor chains of cytochrome bc_1 in all those mutants proceeded from the primary electron donor (QH_2 in the Q_o site) to the final electron acceptor (Q or SQ in the Q_i site) at physiologically and mechanistically competent rates, although changes in $\Delta E_{m_}$b affected equilibrium levels of partial reactions in the coupled electron transfer chains. Clearly, these changes did not introduce any significant barrier to electron transfer from donor to final acceptor. It thus appears that cytochrome bc_1 can accommodate large changes in $\Delta E_{m_}$b without hampering catalysis, as long as these changes do not impose overly endergonic steps on the route of electron transfer from substrate to product. The previously reported moderate decrease in E_m for heme b_H in yeast cytochrome bc_1 falls into this category of changes, *i.e.* ones not imposing overly endergonic steps, and thus, consistent with our observations, did not affect significantly the measured turnover rate of the enzyme (20).

Considering the direction of electron flow and the direction of the gradient of E_m in relation to the vector of the electric membrane potential, four configurations are possible (Fig. 1). In cytochrome bc_1 (11, 12), cytochrome b_6f (37, 38), nitrate reductase A (39, 40), and quinol-fumarate reductase (41, 42), the high potential heme *b* is located at the negative side of the membrane (Fig. 1*a*), which at first would seem to be in line with the concept of the obligatory difference in E_m to overcome membrane potential. However, in formate dehydrogenase N (40, 43, 44) and probably in membrane-bound [Ni-Fe] hydro-

Downloaded from http://www.jbc.org/ by guest on March 13, 2019

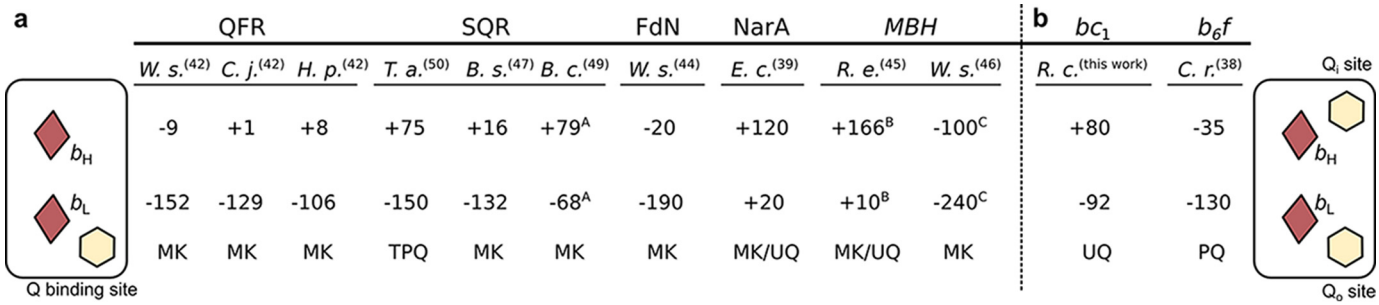

FIGURE 7. **Localization of low and high potential hemes *b* with respect to the quinone binding site in cytochrome *b* subunits of enzymes involved in cross-membrane electron transfer.** *a*, in cytochromes *b* with one Q binding site, low potential heme (b_L) is adjacent to the Q binding site, whereas high potential heme (b_H) faces the opposite side of the membrane. *b*, in cytochromes *bc*, the cytochrome *b* subunit contains two Q binding sites and heme b_L is adjacent to one site (Q_o), whereas heme b_H is adjacent to the other (Q_i). *Brown diamonds*, hemes *b*; *yellow hexagons*, Q binding sites. *Numbers* indicate E_m values (in mV) for pH 7. *Superscripts A*, *B*, and *C* refer to E_m values for pH 7.6, 7.2, and 7.5, respectively. Types of natively used quinones are given below the E_m values. Localization of hemes in membrane-bound [Ni-Fe] hydrogenase (*MBH*) is presumable; thus, its name is given in italic. Protein names abbreviations as in Fig. 1. Other abbreviations as follow: *B. c., Bacillus cereus; B. s., Bacillus subtilis; C. j., Campylobacter jejuni; C. r., Chlamydomonas reinhardtii; E. c., Escherichia coli; H. p., Helicobacter pylori; R. e., Ralstonia eutropha; R. c., Rhodobacter capsulatus; T. a., Thermoplasma acidophilum; W. s., Wolinella succinogenes;* MK, menaquinone; TPQ, thermoplasmaquinone; PQ, plastoquinone; UQ, ubiquinone.

genase (45, 46), the low potential heme is located at the negative side of the membrane, and the electron is transferred against both the electric membrane and the redox potential of hemes *b* (Fig. 1*b*), which remains at odds with the concept presented above. The third possibility found in succinate-quinone reductase (47–50), NADPH oxidase (51), or cytochrome b_{561} family (52–54) is simply an inversion of the case in Fig. 1*a* with electron transfer from high to low potential facilitated by the presence of electric membrane potential (Fig. 1*c*). The fourth possibility (Fig. 1*d*) perhaps concerns proton motive force-driven electron transfer in thiosulfate reductase, if heme b_L in this enzyme is located close to the menaquinone binding site, as in formate dehydrogenase N (which seems likely, based on sequence similarities between the cytochrome *b* subunits of these complexes) (55).

The occurrence of all these configurations suggests that there is no a universal rule for the arrangement of E_m values of hemes *b* among various transmembrane cytochromes *b*. This, however, becomes understandable in light of our observation that large $\Delta E_{m\_}b$ and fine tuning of E_m values of hemes *b* of cytochrome bc_1 are not required for efficient cross-membrane electron transfer. Another example of tolerance for changes in $\Delta E_{m\_}b$ for cross-membrane electron transfer concerns *Bacillus subtilis* succinate-quinone reductase. In this case, the mutant with the His-Met ligated heme b_L having the E_m increased by at least 100 mV is expected to diminish the barrier for the uphill step of electron transfer from heme b_H to heme b_L (Fig. 1*c*) but, at the same time, to introduce a barrier for electron transfer from heme b_L to menaquinone. However, such modification, despite lowered enzymatic activity, did not eliminate the function of the enzyme *in vivo*. Furthermore, its activity to reduce ubiquinone was not significantly affected (48).

Extrapolating all these observations to other cytochromes *b*, it can be proposed that, in all those proteins, hemes *b* simply act as electronic connectors for the catalytic sites with no fine tuning in $\Delta E_{m\_}b$ required for efficient electron transfer. It follows that the existence of $\Delta E_{m\_}b$ in transmembrane embedded hemes *b* is not an element in the control of electron flow across the membrane. Rather, it may be a consequence of a higher probability of coexistence of two cofactors having different E_m in comparison to the case when the two cofactors have similar E_m. Intriguingly, we found one resemblance for enzymes with one quinone binding site: from two hemes *b* of different potentials, the one with the lower potential is adjacent to the quinone binding site (Fig. 7) (38, 39, 42, 44–47, 49, 50). Further studies are required to verify whether this has any functional relevance or is just a consequence of structural constraints. Nevertheless, this resemblance may be useful in predicting the location of low and high potential heme *b* in quinol-binding cytochromes, for which such assignments are yet to be made.

The demonstrated robustness of cytochrome *b* to changes in ligation pattern and associated changes in $\Delta E_{m\_}b$ raises an interesting question as to whether variation in the heme ligation patterns exists in natural membrane proteins of similar design and/or function. Such variation is evident in the group of cytochromes *c* for which bis-His (4, 56, 57), His-Met (4, 56, 57), His-Lys (58), His-Cys (59–61), or even His-Tyr (62, 63) patterns ligating heme iron are observed. However, in most known cytochromes *c*, the heme binding domains are water-soluble or solvent-exposed (so far, the heme c_x from cytochrome b_6 is the only known exception (5, 64, 65)), whereas in cytochromes *b* these domains can be located either in membrane or in aqueous phase (5). It may seem that the location of the heme binding motifs outside the membrane environment is one of the factors increasing structural flexibility to accommodate diverse heme ligation. Indeed, all rare cases of His-Met (66, 67), Lys-Met (68), or bis-Met (69, 70) ligations in cytochromes *b* are relevant only to water-soluble domains. In fact, to our knowledge, no cases have been reported so far of Met or Lys serving naturally as axial ligands for hemes bound within the integral membrane proteins.

However, our Lys mutants prove that His-Lys ligation for hemes *b* can occur within the transmembrane helix bundle of cytochrome *b*, yielding functional hemes that contain a low spin form of iron ion. Notably, the H212K mutant was originally isolated as a reversion for H212N, the so-called heme b_H knockout, with impaired electron transfer at the level of the heme b_H/Q_i site. Likewise, the His-Met heme *b* mutant of *B. subtilis* succinate-quinone reductase was isolated as a reversion of nonfunctional Leu mutant (48). This all indicates that an assembly

Downloaded from http://www.jbc.org/ by guest on March 13, 2019

of functionally active low spin heme *b* present within the transmembrane segment of the protein and coordinated by His and Lys or Met is feasible from a protein engineering perspective. If this is the case, one should expect that there are natural cases of His-Lys and His-Met ligation patterns for membranous heme proteins (71) that still await identification, especially because the range of scrutinized heme proteins is currently continuously widening.

Author Contributions—S. P. performed most of the biochemical and spectroscopic experiments and analyzed data; P. K. performed light-induced electron transfer measurements; E. C. constructed mutants and contributed preliminary results; A. B. performed enzymatic activity assays; and S. P., M. S., and A. O. designed the experiments, interpreted the data, and cowrote the paper. All authors reviewed the results and approved the final version of the manuscript.

Acknowledgments—We thank Dr. Wolfgang Nitschke for useful discussions and Dr. Robert Ekiert for technical assistance.

References

1. Wallace, C. J., and Clark-Lewis, I. (1992) Functional role of heme ligation in cytochrome *c*. *J. Biol. Chem.* **267,** 3852–3861
2. Battistuzzi, G., Borsari, M., Cowan, J. A., Ranieri, A., and Sola, M. (2002) Control of cytochrome *c* redox potential: axial ligation and protein environment effects. *J. Am. Chem. Soc.* **124,** 5315–5324
3. Mao, J., Hauser, K., and Gunner, M. R. (2003) How cytochromes with different folds control heme redox potentials. *Biochemistry* **42,** 9829–9840
4. Fufezan, C., Zhang, J., and Gunner, M. R. (2008) Ligand preference and orientation in *b*- and *c*-type heme-binding proteins. *Proteins* **73,** 690–704
5. Koch, H.-G., and Schneider, D. (2007) Folding, assembly, and stability of transmembrane cytochromes. *Curr. Chem. Biol.* **1,** 59–74
6. Volkmer, T., Becker, C., Prodöhl, A., Finger, C., and Schneider, D. (2006) Assembly of a transmembrane b-type cytochrome is mainly driven by transmembrane helix interactions. *Biochim. Biophys. Acta* **1758,** 1815–1822
7. Berry, E. A., and Walker, F. A. (2008) Bis-histidine-coordinated hemes in four-helix bundles: how the geometry of the bundle controls the axial imidazole plane orientations in transmembrane cytochromes of mitochondrial complexes II and III and related proteins. *J. Biol. Inorg. Chem.* **13,** 481–498
8. Robertson, D. E., Farid, R. S., Moser, C. C., Urbauer, J. L., Mulholland, S. E., Pidikiti, R., Lear, J. D., Wand, A. J., DeGrado, W. F., and Dutton, P. L. (1994) Design and synthesis of multi-haem proteins. *Nature* **368,** 425–432
9. Koder, R. L., Anderson, J. L., Solomon, L. A., Reddy, K. S., Moser, C. C., and Dutton, P. L. (2009) Design and engineering of an O_2 transport protein. *Nature* **458,** 305–309
10. Farid, T. A., Kodali, G., Solomon, L. A., Lichtenstein, B. R., Sheehan, M. M., Fry, B. A., Bialas, C., Ennist, N. M., Siedlecki, J. A., Zhao, Z., Stetz, M. A., Valentine, K. G., Anderson, J. L., Wand, A. J., Discher, B. M., Moser, C. C., and Dutton, P. L. (2013) Elementary tetrahelical protein design for diverse oxidoreductase functions. *Nat. Chem. Biol.* **9,** 826–833
11. Xia, D., Esser, L., Tang, W.-K., Zhou, F., Zhou, Y., Yu, L., and Yu, C.-A. (2013) Structural analysis of cytochrome bc_1 complexes: implications to the mechanism of function. *Biochim. Biophys. Acta* **1827,** 1278–1294
12. Sarewicz, M., and Osyczka, A. (2015) Electronic connection between the quinone and cytochrome *c* redox pools and its role in regulation of mitochondrial electron transport and redox signaling. *Physiol. Rev.* **95,** 219–243
13. Swierczek, M., Cieluch, E., Sarewicz, M., Borek, A., Moser, C. C., Dutton, P. L., and Osyczka, A. (2010) An electronic bus bar lies in the core of cytochrome bc_1. *Science* **329,** 451–454
14. Lanciano, P., Lee, D.-W., Yang, H., Darrouzet, E., and Daldal, F. (2011) Intermonomer electron transfer between the low-potential *b* hemes of cytochrome bc_1. *Biochemistry* **50,** 1651–1663
15. Lanciano, P., Khalfaoui-Hassani, B., Selamoglu, N., and Daldal, F. (2013) Intermonomer electron transfer between the *b* hemes of heterodimeric cytochrome bc_1. *Biochemistry* **52,** 7196–7206
16. Ekiert, R., Czapla, M., Sarewicz, M., and Osyczka, A. (2014) Hybrid fusions show that inter-monomer electron transfer robustly supports cytochrome bc_1 function *in vivo*. *Biochem. Biophys. Res. Commun.* **451,** 270–275
17. Shinkarev, V. P., Crofts, A. R., and Wraight, C. A. (2001) The electric field generated by photosynthetic reaction center induces rapid reversed electron transfer in the bc_1 complex. *Biochemistry* **40,** 12584–12590
18. Nicholls, D. G., and Ferguson, S. J. (2013) *Bioenergetics*, 4th Ed., Academic Press, Amsterdam
19. Brasseur, G., Sariba, A. S., and Daldal, F. (1996) A compilation of mutations located in the cytochrome *b* subunit of the bacterial and mitochondrial bc_1 complex. *Biochim. Biophys. Acta* **1275,** 61–69
20. Rotsaert, F. A., Covian, R., and Trumpower, B. L. (2008) Mutations in cytochrome *b* that affect kinetics of the electron transfer reactions at center N in the yeast cytochrome bc_1 complex. *Biochim. Biophys. Acta* **1777,** 239–249
21. Yun, C. H., Crofts, A. R., and Gennis, R. B. (1991) Assignment of the histidine axial ligands to the cytochrome b_H and cytochrome b_L components of the bc_1 complex from *Rhodobacter sphaeroides* by site-directed mutagenesis. *Biochemistry* **30,** 6747–6754
22. Osyczka, A., Moser, C. C., Daldal, F., and Dutton, P. L. (2004) Reversible redox energy coupling in electron transfer chains. *Nature* **427,** 607–612
23. Atta-Asafo-Adjei, E., and Daldal, F. (1991) Size of the amino acid side chain at position 158 of cytochrome *b* is critical for an active cytochrome bc_1 complex and for photosynthetic growth of *Rhodobacter capsulatus*. *Proc. Natl. Acad. Sci. U.S.A.* **88,** 492–496
24. Cieluch, E., Pietryga, K., Sarewicz, M., and Osyczka, A. (2010) Visualizing changes in electron distribution in coupled chains of cytochrome bc_1 by modifying barrier for electron transfer between the FeS cluster and heme c_1. *Biochim. Biophys. Acta* **1797,** 296–303
25. Czapla, M., Borek, A., Sarewicz, M., and Osyczka, A. (2012) Fusing two cytochromes *b* of *Rhodobacter capsulatus* cytochrome bc_1 using various linkers defines a set of protein templates for asymmetric mutagenesis. *Protein Eng. Des. Sel.* **25,** 15–25
26. Valkova-Valchanova, M. B., Saribas, A. S., Gibney, B. R., Dutton, P. L., and Daldal, F. (1998) Isolation and characterization of a two-subunit cytochrome *b*-c_1 subcomplex from *Rhodobacter capsulatus* and reconstitution of its ubihydroquinone oxidation (Q_o) site with purified Fe-S protein subunit. *Biochemistry* **37,** 16242–16251
27. Czapla, M., Borek, A., Sarewicz, M., and Osyczka, A. (2012) Enzymatic activities of isolated cytochrome bc_1-like complexes containing fused cytochrome *b* subunits with asymmetrically inactivated segments of electron transfer chains. *Biochemistry* **51,** 829–835
28. Osyczka, A., Dutton, P. L., Moser, C. C., Darrouzet, E., and Daldal, F. (2001) Controlling the functionality of cytochrome c_1 redox potentials in the *Rhodobacter capsulatus* bc_1 complex through disulfide anchoring of a loop and a b-branched amino acid near the heme-ligating methionine. *Biochemistry* **40,** 14547–14556
29. Dutton, P. L. (1978) Redox potentiometry: determination of midpoint potentials of oxidation-reduction components of biological electron transfer systems. *Methods Enzymol.* **54,** 411–435
30. Sarewicz, M., Dutka, M., Pintscher, S., and Osyczka, A. (2013) Triplet state of the semiquinone-Rieske cluster as an intermediate of electronic bifurcation catalyzed by cytochrome bc_1. *Biochemistry* **52,** 6388–6395
31. Finnegan, M. G., Knaff, D. B., Qin, H., Gray, K. A., Daldal, F., Yu, L., Yu, C. A., Kleis-San Francisco, S., and Johnson, M. K. (1996) Axial heme ligation in the cytochrome bc_1 complexes of mitochondrial and photosynthetic membranes. A near-infrared magnetic circular dichroism and electron paramagnetic resonance study. *Biochim. Biophys. Acta* **1274,** 9–20
32. Zoppellaro, G., Bren, K. L., Ensign, A. A., Harbitz, E., Kaur, R., Hersleth, H.-P., Ryde, U., Hederstedt, L., and Andersson, K. K. (2009) Studies of ferric heme proteins with highly anisotropic/highly axial low spin ($S = 1/2$) electron paramagnetic resonance signals with *bis*-histidine and histi-

Downloaded from http://www.jbc.org/ by guest on March 13, 2019

dine-methionine axial iron coordination. *Biopolymers* **91,** 1064–1082
33. Robertson, D. E., Ding, H., Chelminski, P. R., Slaughter, C., Hsu, J., Moomaw, C., Tokito, M., Daldal, F., and Dutton, P. L. (1993) Hydroubiquinone-cytochrome c_2 oxidoreductase from *Rhodobacter capsulatus*: definition of a minimal, functional isolated preparation. *Biochemistry* **32,** 1310–1317
34. Takamiya, K. I., and Dutton, P. L. (1979) Ubiquinone in *Rhodopseudomonas sphaeroides*: some thermodynamic properties. *Biochim. Biophys. Acta* **546,** 1–16
35. Zhang, H., Chobot, S. E., Osyczka, A., Wraight, C. A., Dutton, P. L., and Moser, C. C. (2008) Quinone and non-quinone redox couples in complex III. *J. Bioenerg. Biomembr.* **40,** 493–499
36. Osyczka, A., Moser, C. C., and Dutton, P. L. (2005) Fixing the Q cycle. *Trends Biochem. Sci.* **30,** 176–182
37. Saif Hasan, S., Yamashita, E., and Cramer, W. A. (2013) Transmembrane signaling and assembly of the cytochrome b_6f-lipidic charge transfer complex. *Biochim. Biophys. Acta* **1827,** 1295–1308
38. Alric, J., Pierre, Y., Picot, D., Lavergne, J., and Rappaport, F. (2005) Spectral and redox characterization of the heme c_i of the cytochrome b_6f complex. *Proc. Natl. Acad. Sci. U.S.A.* **102,** 15860–15865
39. Rothery, R. A., Blasco, F., Magalon, A., and Weiner, J. H. (2001) The diheme cytochrome *b* subunit (NarI) of *Escherichia coli* nitrate reductase A (NarGHI): structure, function, and interaction with quinols. *J. Mol. Microbiol. Biotechnol.* **3,** 273–283
40. Jormakka, M., Byrne, B., and Iwata, S. (2003) Protonmotive force generation by a redox loop mechanism. *FEBS Lett.* **545,** 25–30
41. Haas, A. H., and Lancaster, C. R. (2004) Calculated coupling of transmembrane electron and proton transfer in dihemic quinol:fumarate reductase. *Biophys. J.* **87,** 4298–4315
42. Mileni, M., MacMillan, F., Tziatzios, C., Zwicker, K., Haas, A. H., Mäntele, W., Simon, J., and Lancaster, C. R. (2006) Heterologous production in *Wolinella succinogenes* and characterization of the quinol:fumarate reductase enzymes from *Helicobacter pylori* and *Campylobacter jejuni*. *Biochem. J.* **395,** 191–201
43. Jormakka, M., Törnroth, S., Byrne, B., and Iwata, S. (2002) Molecular basis of proton motive force generation: structure of formate dehydrogenase-N. *Science* **295,** 1863–1868
44. Kröger, A., Winkler, E., Innerhofer, A., Hackenberg, H., and Schägger, H. (1979) The formate dehydrogenase involved in electron transport from formate to fumarate in *Vibrio succinogenes*. *Eur. J. Biochem.* **94,** 465–475
45. Frielingsdorf, S., Schubert, T., Pohlmann, A., Lenz, O., and Friedrich, B. (2011) A trimeric supercomplex of the oxygen-tolerant membrane-bound [NiFe]-hydrogenase from *Ralstonia eutropha* H16. *Biochemistry* **50,** 10836–10843
46. Gross, R., Pisa, R., Sänger, M., Lancaster, C. R., and Simon, J. (2004) Characterization of the menaquinone reduction site in the diheme cytochrome *b* membrane anchor of *Wolinella succinogenes* NiFe-hydrogenase. *J. Biol. Chem.* **279,** 274–281
47. Hägerhäll, C., Fridén, H., Aasa, R., and Hederstedt, L. (1995) Transmembrane topology and axial ligands to hemes in the cytochrome *b* subunit of *Bacillus subtilis* succinate:menaquinone reductase. *Biochemistry* **34,** 11080–11089
48. Matsson, M., Tolstoy, D., Aasa, R., and Hederstedt, L. (2000) The distal heme center in *Bacillus subtilis* succinate:quinone reductase is crucial for electron transfer to menaquinone. *Biochemistry* **39,** 8617–8624
49. García, L. M., Contreras-Zentella, M. L., Jaramillo, R., Benito-Mercadé, M. C., Mendoza-Hernández, G., del Arenal, I. P., Membrillo-Hernández, J., and Escamilla, J. E. (2008) The succinate:menaquinone reductase of *Bacillus cereus*: characterization of the membrane-bound and purified enzyme. *Can. J. Microbiol.* **54,** 456–466
50. Gärtner, P. (1991) Characterization of a quinole-oxidase activity in crude extracts of *Thermoplasma acidophilum* and isolation of an 18-kDa cytochrome. *Eur. J. Biochem.* **200,** 215–222
51. Yu, L., Quinn, M. T., Cross, A. R., and Dinauer, M. C. (1998) Gp91phox is the heme binding subunit of the superoxide-generating NADPH oxidase. *Proc. Natl. Acad. Sci. U.S.A.* **95,** 7993–7998
52. Desmet, F., Bérczi, A., Zimányi, L., Asard, H., and Van Doorslaer, S. (2011) Axial ligation of the high-potential heme center in an *Arabidopsis* cytochrome b_{561}. *FEBS Lett.* **585,** 545–548
53. Kamensky, Y., Liu, W., Tsai, A.-L., Kulmacz, R. J., and Palmer, G. (2007) Axial ligation and stoichiometry of heme centers in adrenal cytochrome b_{561}. *Biochemistry* **46,** 8647–8658
54. Lu, P., Ma, D., Yan, C., Gong, X., Du, M., and Shi, Y. (2014) Structure and mechanism of a eukaryotic transmembrane ascorbate-dependent oxidoreductase. *Proc. Natl. Acad. Sci. U.S.A.* **111,** 1813–1818
55. Stoffels, L., Krehenbrink, M., Berks, B. C., and Unden, G. (2012) Thiosulfate reduction in *Salmonella enterica* is driven by the proton motive force. *J. Bacteriol.* **194,** 475–485
56. Bewley, K. D., Ellis, K. E., Firer-Sherwood, M. A., and Elliott, S. J. (2013) Multi-heme proteins: nature's electronic multi-purpose tool. *Biochim. Biophys. Acta* **1827,** 938–948
57. Bertini, I., Cavallaro, G., and Rosato, A. (2006) Cytochrome *c*: occurrence and functions. *Chem. Rev.* **106,** 90–115
58. Rodrigues, M. L., Oliveira, T. F., Pereira, I. A., and Archer, M. (2006) X-ray structure of the membrane-bound cytochrome *c* quinol dehydrogenase NrfH reveals novel haem coordination. *EMBO J.* **25,** 5951–5960
59. Kappler, U., Aguey-Zinsou, K.-F., Hanson, G. R., Bernhardt, P. V., and McEwan, A. G. (2004) Cytochrome c_{551} from *Starkeya novella*: characterization, spectroscopic properties, and phylogeny of a diheme protein of the SoxAX family. *J. Biol. Chem.* **279,** 6252–6260
60. Kilmartin, J. R., Maher, M. J., Krusong, K., Noble, C. J., Hanson, G. R., Bernhardt, P. V., Riley, M. J., and Kappler, U. (2011) Insights into structure and function of the active site of SoxAX cytochromes. *J. Biol. Chem.* **286,** 24872–24881
61. Suga, M., Lai, T. L., Sugiura, M., Shen, J. R., and Boussac, A. (2013) Crystal structure at 1.5Å resolution of the PsbV2 cytochrome from the cyanobacterium *Thermosynechococcus elongatus*. *FEBS Lett.* **587,** 3267–3272
62. Jensen, L. M., Meharenna, Y. T., Davidson, V. L., Poulos, T. L., Hedman, B., Wilmot, C. M., and Sarangi, R. (2012) Geometric and electronic structures of the His–Fe(IV)=O and His–Fe(IV)–Tyr hemes of MauG. *J. Biol. Inorg. Chem.* **17,** 1241–1255
63. Jensen, L. M., Sanishvili, R., Davidson, V. L., and Wilmot, C. M. (2010) *In crystallo* posttranslational modification within a MauG/pre-methylamine dehydrogenase complex. *Science* **327,** 1392–1394
64. Kurisu, G., Zhang, H., Smith, J. L., and Cramer, W. A. (2003) Structure of the cytochrome b_6f complex of oxygenic photosynthesis: tuning the cavity. *Science* **302,** 1009–1014
65. Stroebel, D., Choquet, Y., Popot, J.-L., and Picot, D. (2003) An atypical haem in the cytochrome b_6f complex. *Nature* **426,** 413–418
66. Mathews, F. S., Bethge, P. H., and Czerwinski, E. W. (1979) The structure of cytochrome b562 from *Escherichia coli* at 2.5 A resolution. *J. Biol. Chem.* **254,** 1699–1706
67. Rotsaert, F. A., Hallberg, B. M., de Vries, S., Moenne-Loccoz, P., Divne, C., Renganathan, V., and Gold, M. H. (2003) Biophysical and structural analysis of a novel heme *b* iron ligation in the flavocytochrome cellobiose dehydrogenase. *J. Biol. Chem.* **278,** 33224–33231
68. Kloer, D. P., Hagel, C., Heider, J., and Schulz, G. E. (2006) Crystal structure of ethylbenzene dehydrogenase from *Aromatoleum aromaticum*. *Structure* **14,** 1377–1388
69. Cheesman, M. R., Thomson, A. J., Greenwood, C., Moore, G. R., and Kadir, F. (1990) Bis-methionine axial ligation of haem in bacterioferritin from *Pseudomonas aeruginosa*. *Nature* **346,** 771–773
70. Ran, Y., Zhu, H., Liu, M., Fabian, M., Olson, J. S., Aranda, R., 4th, Phillips, G. N., Jr., Dooley, D. M., and Lei, B. (2007) Bis-methionine ligation to heme iron in the streptococcal cell surface protein Shp facilitates rapid hemin transfer to HtsA of the HtsABC transporter. *J. Biol. Chem.* **282,** 31380–31388
71. Bérczi, A., Desmet, F., Van Doorslaer, S., and Asard, H. (2010) Spectral characterization of the recombinant mouse tumor suppressor 101F6 protein. *Eur. Biophys. J.* **39,** 1129–1142

Downloaded from http://www.jbc.org/ by guest on March 13, 2019